

¹ **Dynamic spatiotemporal modeling of a habitat defining plant
species to support wildlife management at regional scales**

³ ANDREW T. TREDENNICK^{*1}, ADRIAN P. MONROE², THOMAS PREBYL¹, JOHN LOMBARDI¹, &

⁴ CAMERON L. ALDRIDGE³

⁵ *¹Western EcoSystems Technology, Inc., Laramie, WY*

⁶ *²Fort Collins Science Center, U.S. Geological Survey, Fort Collins, CO*

⁷ *³Natural Resource Ecology Laboratory and Department of Ecosystem Science and Sustainability, Colorado*

⁸ *State University, Fort Collins, CO, in cooperation with US Geological Survey, Fort Collins Science Center,*

⁹ *Fort Collins, CO*

¹⁰ **Open Research Statement**

¹¹ Data and code are provided as private-for-peer review (shared publicly in a repository: <https://github.com/WEST-Inc/sageCastR>). Data and code will be archived on Zenodo upon acceptance.

^{*}Corresponding author: *email, atredenn@gmail.com; phone, 970-443-1599*; Current affiliation, Metrum Research Group

13 **Abstract**

14 Sagebrush (*Artemisia* spp.) ecosystems provide critical habitat for the near-threatened Greater
15 sage-grouse (*Centrocercus urophasianus*). Thus, future loss of sagebrush habitat because of land use
16 change and global climate change is of concern. Here we use a dynamic additive spatio-temporal
17 model to estimate the effects of climate on sagebrush cover dynamics at 32 sage-grouse management
18 areas in Wyoming. We use the fitted models to quantify the sensitivity of each management area
19 to precipitation and temperature, and to make probabilistic projections of sagebrush cover from
20 present to 2100 under three climate change scenarios. Global circulation models predict an increase
21 in temperature and no change in precipitation for Wyoming. Sensitivity to climate varied among
22 management areas but the most common response (70% of management areas) was a positive effect
23 of temperature on sagebrush performance. The combination of positive sensitivity to temperature
24 and the predicted increase in temperature under all climate change scenarios resulted in projections
25 of increased sagebrush cover for most management areas. We characterized management areas
26 as “optimal” or “suboptimal” based on the percentage of grid cells in each management area with
27 sagebrush cover exceeding a nesting habitat target value. Only 18% of management areas are
28 projected to switch from being currently optimal to suboptimal in the future. Thirty-five percent of
29 management areas are projected to switch from being suboptimal to optimal. The most common
30 outcome (47%) was for currently suboptimal management areas to remain suboptimal, even though
31 average cover tended to increase in those areas. The direct effects of climate change appear to favor
32 sagebrush performance in the future for most sage-grouse core areas in Wyoming. Our approach is
33 broadly applicable to quantitative climate change assessments where remotely-sensed estimates of
34 habitat-defining vegetation are available.

35 *Key words:* Artemisia, *Centrocercus urophasianus*, *climate change*, *Greater sage-grouse*, *popu-*
36 *lation model*, *remote sensing*, *sagebrush*

37 **Introduction**

38 Environmental management and stewardship requires assessing tradeoffs (Walters and Hilborn 1978,
39 Farber et al. 2006). For example, land managers must consider the long-term impacts of climate
40 change and the near-term impacts of ecosystem degradation (e.g., Nepstad et al. 2008). Because
41 populations, communities, and ecosystems are not static, using the current status of an ecosystem to
42 make management decisions may not be optimal (Boettiger et al. 2016). A better approach is to
43 consider the past, current, and future status of ecosystems. Doing so requires projections of how an
44 ecosystem might respond to future stressors and conditions (Clark et al. 2001, Dietze et al. 2018).

45 Infrastructure development indirectly and negatively affects species through habitat loss and
46 transformation, which is a major driver of biodiversity loss (Sala et al. 2000, Cardinale et al. 2012,
47 Powers and Jetz 2019). Wildlife management often requires assessing tradeoffs between the benefits
48 of development and the costs of habitat loss or degradation (McShane et al. 2011). To assess that
49 tradeoff, managers often identify areas of high and low quality habitat. Low quality habitat is then
50 preferred for habitat alteration. But habitat quality is not static and global climate change has the
51 potential alter the trajectory of an ecosystem. Some currently high quality habitat (for a particular
52 species) might quickly change if on a range edge while lower quality habitat in the middle of the
53 range might maintain its general structure and function longer (Amburgey et al. 2018). Habitat on
54 the edge of an ecosystem's range might also improve. For example, warming temperatures could
55 benefit some plants at the cold edge of their range (Kleinhesselink and Adler 2018). Thus, climate
56 change adds a new dimension to habitat assessments, where we are not only concerned about the
57 current status of habitat but also what that habitat might look like 30 to 100 years in the future.

58 Land management in the western United States focuses on several uses and species, but Greater
59 sage-grouse (*Centrocercus urophasianus*, hereafter “sage-grouse”) typically drive the conversation
60 in sagebrush dominated ecosystems. Sage-grouse are a protected species in Canada (Species at Risk
61 Act [S.C. 2002, c. 29], <https://laws-lois.justice.gc.ca/eng/acts/S-15.3/>) and are listed as “warranted,
62 but precluded” for listing under the United States Endangered Species Act of 1973 (U.S. Fish
63 and Wildlife Service [USFWS] 2010). Sagebrush ecosystems provide critical habitat for Greater

64 sage-grouse and other sagebrush obligate species (Carlisle and Chalfoun 2020). Conservation of
65 sagebrush ecosystems is primarily aimed at keeping sage-grouse off the endangered species list
66 but sagebrush conservation will benefit other species, too (Rowland et al. 2006, Smith et al. 2019,
67 Pilliod et al. 2020). In response to declining sage-grouse populations, the Wyoming Game and Fish
68 Department has delineated 32 sage-grouse core areas, covering approximately 15 million acres of
69 sage-grouse habitat (State of Wyoming 2015). The stated goal of the Core Area strategy is “...to
70 minimize future disturbance by co-locating proposed disturbances within area already disturbed or
71 naturally unsuitable” (State of Wyoming 2015). Sage-grouse populations are active in all core areas
72 and most maintain stable populations (Edmunds et al. 2018), though populations outside of these
73 core areas are not performing the same.

74 In Wyoming, many of the landscapes with the highest potential for wind energy also support
75 critical sage-grouse habitat in the form of sagebrush dominated ecosystems. This presents a
76 challenge to land management: Should land be prioritized for sage-grouse conservation or renewable
77 energy development? Renewable energy infrastructure that can mitigate the impacts of climate
78 change could benefit sage-grouse in the long run. Therefore, it is critical to understand the potential
79 impacts of climate change across sagebrush landscapes because some areas may become less
80 beneficial to sage-grouse due to climate change, making those areas attractive for development of
81 renewable energy infrastructure, potentially minimizing such conflicts. Considering how climate
82 change impacts whether a sage-grouse core area is or will be “naturally unsuitable” clearly falls
83 within the scope of the Core Area strategy. More broadly, assessing current and future habitat
84 suitability *vis-a-vis* species of concern is essential as we face difficult and inevitable trade-offs
85 between land preservation and land-use to combat climate change.

86 The sagebrush biome, as a whole, is in peril (Palmquist et al. 2021). But Wyoming is thought to
87 be a stronghold where sagebrush will persist and possibly thrive in the future, especially compared
88 to other parts of its range (Palmquist et al. 2021). In part, this is because the sagebrush biome
89 in Wyoming has been less susceptible to cheatgrass (*Bromus tectorum*) invasion, compared to
90 other parts of the sagebrush biome (Pastick et al. 2021). Cheatgrass invasion, and the subsequent

91 cheatgrass-fire feedback cycle, is the main driver of the loss of sagebrush cover across most of
92 sagebrush's range (Balch et al. 2013). Because susceptibility to cheatgrass invasion is an indirect
93 effect of climate change (Chambers et al. 2007, Bradley 2009), and because cheatgrass invasion
94 has not been as dramatic in Wyoming, it stands to reason that the direct effects of climate change
95 have important implications in Wyoming. This is especially true if increases in sagebrush cover due
96 to climate change can inhibit cheatgrass invasion. Indeed, recent modeling suggests that warming
97 temperatures will benefit sagebrush more than cheatgrass at high elevation sites, assuming fire is
98 limited (Palmquist et al. 2021). Therefore, this paper focuses on modeling the direct effects of
99 climate on sagebrush cover change.

100 Here we describe a computationally efficient Bayesian spatiotemporal modeling approach for
101 making probabilistic projections of sagebrush cover dynamics under the direct effects of climate
102 change in Wyoming, USA using remotely sensed cover estimates. A key feature of our approach is
103 using the probabilistic projections to evaluate specific management targets for sagebrush cover in
104 sage-grouse core areas. Our approach is applicable to diverse situations where clear management
105 targets exist and spatiotemporal data are available to train probabilistic models.

106 Materials and Methods

107 Data

108 Remotely-sensed time series

109 We used the Rangeland Condition, Monitoring, Assessment, and Projection (RCMAP) data product
110 from the National Land Cover Database (NLCD), a product of the Multi-Resolution Land Charac-
111 teristics Consortium (Rigge et al. 2020). We downloaded the “NLCD BIT Sagebrush Fractional
112 Component” estimates for each year from 1985 to 2018, subset the data to the Wyoming Sage-grouse
113 core areas, and then resampled the data up to 100-meter resolution using the mean to aggregate
114 cover across 30-meter grid cells. We resampled the data to make the analysis computationally

115 tractable: decreasing the spatial resolution resulted in fewer cells of data per year and thus reduced
116 the total size of the observed data. Time series of cover are shown in Fig. 1. There are no data for
117 2012, which we handled naively by letting 2011 be the “lag cover year” for 2013.

118 [Figure 1 about here.]

119 Climate covariates

120 We downloaded historical climate estimates from PRISM (<http://prism.oregonstate.edu/>), with
121 spatial extents that matched the sage-grouse core areas. From these estimates, we calculated two
122 climate covariates: 1) average spring-through-summer temperature and 2) average spring-through-
123 summer precipitation. We defined spring-through-summer as March 1 through August 31 for each
124 year. We decided on the two covariates based on our previous work (Tredennick et al. 2016) and
125 more recent work by Kleinhesselink and Adler (2018). Previous modeling of sagebrush dynamics in
126 Wyoming and across the sagebrush range used “lagged covariates” like precipitation in the year prior
127 to an observed transition. We do not use lagged covariates here because exploratory work suggests
128 that lagged covariates result in correlated and confounded parameter estimates (Kleinhesselink pers.
129 comm.).

130 Climate projections

131 We used climate projections from Global Circulation Models (GCMs) that contributed to the
132 CMIP6 project (Eyring et al. 2016). Groups that contributed to CMIP6 provided output from
133 several experimental conditions. We used three common experimental conditions for generating
134 future projections under different shared socio-economic pathways (SSPs): ssp126 (low future
135 carbon emissions), ssp245 (intermediate future carbon emissions), and ssp585 (high future carbon
136 emissions) (see Eyring et al. (2016) for more details). GCM ouputs were downloaded from
137 Lawrence Livermore National Library archives of CMIP6 model simulations and projections. We
138 used the `esfg_query` function from the `epwshiftr` R package (Jia and Chong 2020) the query the
139 database and download the data. In total, we compiled future climate projections from 18 GCMs.

¹⁴⁰ We applied a bias correction to the GCM values by shifting the means of GCM projections in
¹⁴¹ reference to PRISM data from the historical time period.

¹⁴² GCM projections vary in their accuracy depending on location. Therefore, we weighted each of
¹⁴³ the GCMs by their ability to reproduce observed data (Rupp et al. 2013). To evaluate each GCM
¹⁴⁴ we compared historical projections (1985 - 2018) from each GCM to PRISM data for the same time
¹⁴⁵ span and geographic area. For each year we resampled the historic GCM raster data to match the
¹⁴⁶ spatial resolution of the PRISM data and extracted values for the two climate variables (average
¹⁴⁷ spring-through-summer temperature and average spring-through-summer precipitation) for each
¹⁴⁸ sage-grouse core area, then calculated the mean climate variable value across all core areas.

¹⁴⁹ Following Rupp et al. (2013), we calculated the relative error (E^*) across the entire time span
¹⁵⁰ for both climate variables and for each GCM as

$$E_{i,j}^* = \frac{E_{i,j} - \min(E_j)}{\max(E_j) - \min(E_j)} \quad (1)$$

¹⁵¹ where i indexes the variable (temperature or precipitation) and j indexes the GCM. $E_{i,j}$ is the mean
¹⁵² absolute error, calculated as $E_{i,j} = \frac{\sum_{k=1}^K |x_{i,j,k} - z_{i,j,k}|}{K}$, where x is the observed value from PRISM and z
¹⁵³ is the value from the GCM and k indexes the observation (an annual mean value for a particular
¹⁵⁴ year), and K is the total number of observations. Last, we averaged the E^* values across the two
¹⁵⁵ variables (temperature and precipitation) to arrive at a single relative error value for each of the J
¹⁵⁶ GCMs: $E_j^* = (\sum_{i=1}^N E_{i,j}^*) / N$, where $N = 2$ is the total number of variables. The resulting relative
¹⁵⁷ errors for each GCM were used as weights ($w_j = 1 - E_j^*$) when making projections of sagebrush
¹⁵⁸ dynamics forced by the GCM output. Specifically, the projected time series of weather we used
¹⁵⁹ under each scenario is the weighted average of all GCMs, with w_j being the weight for each GCM j .

160 **Model**

161 **Dynamic additive spatio-temporal model for sagebrush cover**

162 We used a descriptive, dynamic model of sagebrush cover, building on our previous work (Treden-
163 nick et al. 2016) and animal population modeling described by Conn et al. (2015). Our model
164 represents the observed sagebrush cover in cell i of year t ($y_{i,t}$) as arising from a Poisson process
165 with rate $\exp(\mu_{i,t})$:

$$y_{i,t} \sim \text{Poisson}(\exp(\mu_{i,t})). \quad (2)$$

166 The deterministic process model follows the log-transformed version of a Gompertz population
167 growth model, representing $\mu_{i,t}$ as

$$\mu_{i,t} = \beta x'_{i,t} + \gamma_t + w_i \quad (3)$$

168 where β is a vector of regression coefficients, $x_{i,t}$ is a vector of covariates for cell i at time t , γ_t is a
169 temporal random effect, and w_i is a spatial offset for each cell i . The covariate vector $x_{i,t}$ is one row
170 of the design matrix \mathbf{X} , which includes a column of 1s for the intercept, a column of logged lag
171 cover ($\log(y_{t-1})$) values, a column for the precipitation covariate, and a column for the temperature
172 covariate. \mathbf{X} is a $n \times p$ matrix and each row represents a single observation, indexed by time (t , year
173 of observation) and cell (i , spatial location). We added a small offset (0.0001) to all one-year lagged
174 observed percent cover values that occur in the design matrix \mathbf{X} before logging those values so that
175 0 cover values could be included easily.

176 In previous work we estimated the spatial offset using kernel convolution and dimension
177 reduction (Tredennick et al. 2016). Estimating the spatial offset is not strictly necessary because
178 the data represent a full sample of the spatial domain. Here we use an empirical approach to
179 calculate the spatial offset because it substantially reduces computational time and results in a better
180 representation of the spatial variance. We calculated the spatial offset for each grid cell as the
181 difference between the log of the focal mean of a cell over time and the log of mean cover across

182 each complete core area over time. More specifically, we calculated the spatial offset w_i for each
183 cell i in a core area as

$$w_i = \log(\bar{f}_i) - \log(\bar{y}), \quad (4)$$

184 where \bar{y} is the mean cover across all years and cells within the core area and \bar{f}_i is the weighted focal
185 mean of all surrounding cells within a radius r ,

$$\bar{f}_i = \frac{1}{n} \sum_{j=1}^n x_j \times k_j, \quad (5)$$

186 with weights, k_j , defined using an exponential decay function,

$$k_j = \exp\left(\frac{-d_j}{(r \times \frac{1}{3})}\right), \quad (6)$$

187 where d_j is the distance in meters from cell j to focal cell i and n is the total number of cells within
188 the radius r of the focal cell. We defined r as the maximum range of spatial dependence in residuals
189 from a simple generalized linear model (GLM) fit without climate covariates for each core area
190 (Tredennick et al. 2016). The focal function from the **raster** package in R cannot accommodate
191 missing values when calculating a focal mean with custom weights. We pre-filled any cells with
192 missing cover values using a focal mean with equal weight for all cells within the analysis radius
193 r . After calculating \bar{f}_i , all cells that originally had missing cover values were re-set to NA before
194 calculating the final spatial offset value w_i . Missing cover values corresponded to masked areas not
195 defined as “sagebrush” habitat in the RCMAP products.

196 The full Bayesian posterior distribution of the dynamic-additive spatiotemporal model is:

$$\begin{aligned}
[\beta, \gamma, \sigma_\gamma | \mathbf{y}, \mathbf{X}, \mathbf{w}] &\propto \prod_{t=1}^T \prod_{i=1}^N [y_{i,t} | \beta, \gamma, w_i] \\
&\times [\gamma_t | \sigma_\gamma] \\
&\times [\beta] [\sigma_\gamma]. \tag{7}
\end{aligned}$$

197 An attractive feature of the Gompertz population model in log space (Eq. 3) is that equilibrium
 198 abundance is defined as: $\mu' = \beta_1 / (1 - \beta_2)$ (Ives et al. 2003, Kleinhesselink and Adler 2018). Note
 199 that this definition holds when the random effects are centered on 0 and when the covariates are
 200 scaled and centered on 0. Both of these conditions hold in our model. We use equilibrium abundance
 201 (cover, in our case) as a starting point for sensitivity analyses. For example, equilibrium cover across
 202 all cells in a core area is $\bar{y}' = \exp(\mu')$. Equilibrium cover for a particular cell (i) is $y'_i = \exp(\mu' +$
 203 $w_i)$. Equilibrium cover for a particular cell (i) under a climate scenario where the future climate
 204 is 1 standard deviation greater than current climate is $y'_i = \exp(\mu' + w_i + (1 \times \beta_3) + (1 \times \beta_4))$
 205 (Kleinhesselink and Adler 2018). Projections of future cover were initialized with observed cover
 206 in 2018.

207 We used results from Tredennick et al. (2016) to define informative prior distributions for the
 208 intercept (β_1) and density-dependence (β_2) regression parameters in Eq. 3 (Table 1). Vague prior
 209 distributions were assigned to all other parameters (Table 1).

210 [Table 1 about here.]

211 **Model fitting and evaluation**

212 We used Hamiltonian Monte Carlo (HMC) to approximate the posterior distributions of all unknown
 213 parameters. Specifically, we used the Stan software (Stan Development Team 2020) to implement
 214 the HMC algorithm, using the rstan package (Guo et al. 2020) to connect Stan to R. We ran
 215 three chains of 1,000 iterations after a burn-in of 1,000 iterations. Convergence of the MCMC
 216 chains was assessed visually with traceplots and by ensuring that the 95% upper credible interval of

217 scale reduction factors (\hat{R}) were less than 1.1 (Gelman and Rubin 1992, Gelman and Hill 2006).
 218 Convergence diagnostics for the intercept (β_1) and the temporal random effects (γ) were computed
 219 after applying “post-sweeping” to address mixing and convergence problems associated with weak
 220 identifiability (Ogle and Barber 2020).

221 We used a subset of the data to fit the model. We did this to make estimation via MCMC
 222 possible in a reasonable time frame. We extracted a spatially balanced 5% sample of grid cells
 223 from each core area to use for model fitting. We used the function `bas.polygon` from the **SDraw**
 224 R package (McDonald et al. 2020) to sample the grid cells for model fitting. Some core areas (e.g.,
 225 Greater South Pass) were divided into smaller subsets that were fitted independently due to memory
 226 constraints. Core areas that were divided are indicated by having a number next to their name or
 227 abbreviation (e.g., Greater South Pass 1, Greater South Pass 2, etc.). Note that the spatial offsets
 228 for each grid cell i (w_i) were calculated for the entire spatial domain and then we extracted the 5%
 229 sample of all relevant information: cover, lag cover, climate covariates, and the spatial effects for
 230 each selected grid cell.

231 We used posterior predictive checks to calculate Bayesian P values assessing the lack-of-fit
 232 between the model and the data (Hobbs and Hooten 2015, Conn et al. 2018). We simulated
 233 cover data for each cell and year ($y_{i,t}^{\text{new}}$) from the model at each MCMC iteration and used a chi-
 234 square statistic to compare the data (both original and “new” data) to the expected values from the
 235 deterministic regression model. The test statistics were then summed over time and space separately,
 236 yielding test statistics for each cell over years for both the new and original datasets,

$$\tau_i^{\text{new}} = \sum_{t=1}^Y \frac{(y_{i,t}^{\text{new}} - \mu_{i,t})^2}{\mu_{i,t}} \quad (8)$$

237 and

$$\tau_i = \sum_{t=1}^Y \frac{(y_{i,t} - \mu_{i,t})^2}{\mu_{i,t}}, \quad (9)$$

238 and for each year over cells for both the original and new datasets,

$$\tau_t^{\text{new}} = \sum_{i=1}^S \frac{(y_{i,t}^{\text{new}} - \mu_{i,t})^2}{\mu_{i,t}} \quad (10)$$

239 and,

$$\tau_t = \sum_{i=1}^S \frac{(y_{i,t} - \mu_{i,t})^2}{\mu_{i,t}}. \quad (11)$$

240 We then computed Bayesian p-values as the proportion of the total number of MCMC iterations for
241 which $\tau^{\text{new}} > \tau$ for each cell or year. Lastly, we average the Bayesian p-values over years and cells
242 to compute two final p-values to evaluate lack-of-fit: one for lack-of-fit over the spatial dimension
243 (P_B^{space} , averaged over years) and one for lack-of-fit over the temporal dimension (P_B^{time} , averaged
244 over cells). Posterior predictive checks were done using a new spatially balanced sample of the data
245 (i.e., a different sample than used to fit the model).

246 All computations were done in R (R Core Team 2020). We bundled the computer code needed
247 to format data, fit the model, evaluate the model, and project the model forward in an R package
248 called **sageCastR** (<https://github.com/WEST-Inc/sageCastR>). Note that the R package is not a
249 generalizable piece of software; it is a code bundle for this particular project. We also note that
250 fitting the models required a high memory machine and parallel processing. Interested users can
251 modify the code for future research.

252 Model projections

253 We made projections of sagebrush cover in each core area under each of the three climate change
254 scenarios (ssp126, ssp245, and ssp585). Initial conditions were defined as the last year of BIT cover
255 estimates for each core area. Climate covariates for each year were calculated as the weighted
256 averages across the GCMs. The weighted averages for the precipitation and temperature covariates
257 were then scaled using the mean and standard deviation for each covariate from the model fitting
258 stage. This was done independently for each core area and was necessary because we used Z-score

transformed covariates for model fitting. We projected sagebrush cover to the year 2100, using 50 random MCMC parameter sets to approximate the posterior predictive distribution (Hobbs and Hooten 2015). We used 50 posterior parameter sets instead of the full posterior distribution (3000 MCMC parameter sets) to decrease computation time and data storage.

We also used a colonization model when projecting the model forward to avoid local extinction in grid cells. We fit a binomial regression model for each core area to estimate the probability of a grid cell with zero percent cover in year t transitioning to non-zero cover in year $t+1$ (Tredennick et al. 2016). This probability was used in the dynamic projections whenever a grid cell had zero cover to simulate whether the grid cell would stay at zero or increase to non-zero cover. We calculated the average cover in cells that transitioned from zero cover to non-zero cover for each core area. Those values were used in the simulation model as the cover assigned to cells that were simulated to transition from zero cover to non-zero cover.

Our main goal was to evaluate future cover projections relative to specific management targets. We defined two management targets: 1) the percent cover needed at 100-meter resolution to maintain sage-grouse nesting habitat and 2) the percent cover needed at 100-meter resolution to maintain sage-grouse summer habitat. We used the 1985-2018 sagebrush cover rasters (resampled to 100 m resolution) to determine the 95% quantile of the time series for each pixel. This quantile should indicate potential sagebrush cover at each pixel while reducing the influence of temporal anomalies. Then, we divided Wyoming into three regions (southwest, central, and northeast) and determined the median value across all 95% quantiles that intersected either nesting or summer sage-grouse habitat, by region (Fedy et al. 2014). These provided threshold values for nesting and summer habitat that were region-specific yet consistent with thresholds recommended by the Sage-grouse Habitat Assessment Framework: 15-25% cover for nesting and 10-25% cover for summer (Stiver et al. 2015). The threshold values we calculated are provided in the online supporting information.

Based on Fedy et al. (2014), we set our landscape level management goal to be 50% of grid cells in a core area meeting or exceeding the nesting target percent cover value. We defined core areas as “optimal” or “suboptimal” for sage-grouse based on this management goal: optimal = 50%

286 of grid cells meeting or exceeding the nesting target, suboptimal = 50% of grid cells below the
287 nesting target. We further categorized core areas into four groups: 1) areas that were estimated to
288 be optimal in 2019 and are projected to remain optimal by 2100, 2) areas that were estimated to
289 be optimal in 2019 and are projected to become suboptimal by 2100, 3) areas that were estimated
290 to be suboptimal in 2019 and are projected to become optimal by 2100, and 4) areas that were
291 estimated to be suboptimal in 2019 and are projected to remain suboptimal by 2100. Categorization
292 was done assuming the ssp585 climate forcing scenario because observed emissions have most
293 closely followed the modeled emissions of ssp585's precursor (RCP8.5) in the recent past. We
294 used the 2019 model projections as the baseline for categorization rather than observed cover in
295 2018 because the projections have slightly lower spatial variance than the observed data. We used
296 sage-grouse population growth rate estimates from Edmunds et al. (2018) to see whether core
297 areas projected to become optimal or suboptimal have currently declining, stable, or increasing
298 sage-grouse populations.

299 Results

300 Global circulation model rankings and projections

301 Relative errors of the GCMs showed that no single GCM was best at recreating historic temperature
302 and precipitation (Fig. 2A). The best GCM was INM-CM4-8, which had the lowest combined
303 relative error for precipitation and temperature (Fig. 2). The errors in the "Combined" panel are
304 inversely proportional to the weights used when aggregating projections of sagebrush dynamics
305 in the future. Projections based on the INM-CM4-8 future climate covariates will have the most
306 weight and projections based on the SAMO-UNICON model will have the least weight.

307 The amount of spring-through-summer precipitation is not expected to change in Wyoming,
308 according to the GCMs we evaluated (Fig. 2B). Temperature is projected to increase, with the
309 largest increase expected under the ssp585 emissions scenario (Fig. 2B). Average temperature in
310 2080-2100 is projected to be 6.7 degrees Celsius higher than average temperature from 1982-2015

³¹¹ under the ssp585 emissions scenario (Table 2). Interannual variation is not expected to substantially
³¹² increase or decrease over time (Table 2).

³¹³ [Table 2 about here.]

³¹⁴ [Figure 2 about here.]

³¹⁵ Statistical model evaluation

³¹⁶ Convergence diagnostics indicated that all MCMC chains converged on their stationary distributions
³¹⁷ (upper 0.95 quantiles of $\hat{R} < 1.1$ for all parameters; see online supporting information). Most
³¹⁸ Bayesian P -values indicated no lack-of-fit because they were greater than 0.05 and less than 0.95 for
³¹⁹ both the spatial (P_B^{space}) and temporal (P_B^{time}) test statistic P -values. The P_B^{time} value for Elk Basin
³²⁰ West indicated lack-of-fit. The P_B^{space} values for Powder, Sage, Seedskadee, and Uinta indicated
³²¹ lack-of-fit. We do not present any further results on these sites because inference from their models
³²² cannot be trusted (Hobbs and Hooten 2015).

³²³ Parameter estimates

³²⁴ Posterior distributions for all model parameters for each core area are presented in the online
³²⁵ supporting information. The posterior distributions of equilibrium cover ($y' = e^{\beta_1/(1-\beta_2)}$) for each
³²⁶ core area contain the observed mean cover values, except for a few core areas (Fig. 3). Cases where
³²⁷ mean observed cover does not fall within estimated equilibrium cover suggest that climate effects
³²⁸ over the past 30 years or other disturbances not modeled (but potentially reflected in random year
³²⁹ effects) have kept cover from reaching the equilibrium. Climate effects are described as sensitivities
³³⁰ below.

³³¹ [Figure 3 about here.]

³³² [Table 3 about here.]

³³³ **Sensitivities**

³³⁴ All core areas showed some sensitivity to climate drivers (Fig. 4). The majority of core areas had
³³⁵ a positive sensitivity to temperature and negative sensitivity to precipitation ($n = 16$; Fig. 5). The
³³⁶ most consistent pattern was a positive effect of temperature on sagebrush performance ($n = 24$ out
³³⁷ of 34 total [70%]; Figs. 4, 5).

³³⁸ [Figure 4 about here.]

³³⁹ [Figure 5 about here.]

³⁴⁰ Averaging over all the posterior distributions for the precipitation and temperature effects, we
³⁴¹ found that overall average effect of precipitation was negative: mean = -0.036 (pseudo 95% BCI =
³⁴² -0.038, -0.034). The overall average effect of temperature was positive: mean = 0.025 (pseudo 95%
³⁴³ BCI = 0.023, 0.027). Note that we refer to the confidence intervals as “pseudo BCIs” because the
³⁴⁴ average of the posteriors is not strictly the cross-core area posterior distribution. Nonetheless, the
³⁴⁵ average values do inform the general pattern. The variance of the overall average effects should be
³⁴⁶ viewed as the variance of the mean effect, not as the variance of effect sizes across core areas.

³⁴⁷ **Projections**

³⁴⁸ Projections of sagebrush cover into the future are primarily driven by the sensitivity of cover to
³⁴⁹ temperature and the magnitude of temperature change. This is because precipitation is not projected
³⁵⁰ to increase or decrease much in the future in Wyoming (Fig. 2B). Because most core areas had a
³⁵¹ positive sensitivity to temperature, sagebrush cover is projected to increase at most core areas (Fig.
³⁵² 6). Projections of sagebrush cover are similar across GCM scenarios until about mid-century, at
³⁵³ which point ssp585 projections diverge if temperature has a large (positive or negative) effect on
³⁵⁴ interannual changes in sagebrush cover (Fig. 6).

³⁵⁵ More core areas were projected to increase ($n = 21$ for ssp126; $n = 22$ for ssp245 and ssp585)
³⁵⁶ than decrease ($n = 13$ for ssp126; $n = 12$ for ssp245 and ssp585) and the magnitude of increases

357 was greater than decreases for each GCM scenario. For decreases, the median percent difference
358 between average cover in 2018 and average cover in 2100 was -9% for ssp126, -18% for ssp245,
359 and -24% for ssp585. For increases, the median percent difference between average cover in 2018
360 and average cover in 2100 was 17% for ssp126, 34% for ssp245, and 79% for ssp585. The percent
361 differences show that projected increases in sagebrush cover are nearly twice the magnitude of
362 projected decreases for each GCM scenario, on average. Summing across core areas, NA - NA km²
363 of land is projected to experience increases in sagebrush cover on average, depending on GCM
364 scenario. NA - NA km² of land is projected to experience decreases in sagebrush cover on average,
365 depending on GCM scenario.

366 Figure 7 shows projections over time and space for the Salt Wells core area (as an example)
367 under the ssp585 climate forcing scenario. Spatial heterogeneity is maintained because of the spatial
368 offset included in the model, but heterogeneity is smoothed somewhat, resulting in slightly lower
369 spatial variance. Lower spatial variance can impact the calculation of the proportion of grid cells
370 with cover over or under the nesting and summer habitat targets. At this core area, projections show
371 sagebrush declining in most of the area with a hotspot of increasing sagebrush on the western edge
372 (Fig. 7).

373 Notable declines in sagebrush cover are projected for Bear River (BrRv), Elk Basin East (ElBE),
374 Jackson (Jcks), Little Mountain (LttM), and North Gillette (NrthGll) core areas (Fig. 6). These
375 same core areas may become suboptimal for sage-grouse over the long-term, as projections suggest
376 the proportion of cells in Bear River, Little Mountain, and Jackson that exceed the sage-grouse
377 nesting target drop below 50% at some point in the future (Figs. 8 and 9B). Twelve core areas are
378 projected to switch from supoptimal to optimal for sage-grouse by crossing the 50% threshold in
379 the future (Figs. 8 and 9D). The most common projection ($n = 16$) is for currently suboptimal core
380 areas to remain suboptimal, even though most will experience gains in sagebrush cover (Fig. 9).

381 Most sage-grouse population growth rates have confidence intervals that overlap one, indicating
382 a stable population (Fig. 9). However, the mean growth rates suggest that 12 of the 16 core areas
383 projected to remain suboptimal already have declining sage-grouse populations (Fig. 9C). Ten of

³⁸⁴ the 12 core areas projected to switch from suboptimal to optimal have mean sage-grouse population
³⁸⁵ growth rates that are negative (Fig. 9D).

³⁸⁶ [Figure 6 about here.]

³⁸⁷ [Figure 7 about here.]

³⁸⁸ [Figure 8 about here.]

³⁸⁹ [Figure 9 about here.]

³⁹⁰ Discussion

³⁹¹ Projections of sagebrush cover represent the combined effect of sensitivity to the climate drivers
³⁹² and the magnitude of change expected in the climate driver in the future. We found that sagebrush
³⁹³ performance at most core areas showed positive sensitivity to temperature and negative sensitivity
³⁹⁴ to precipitation. Because average temperature is expected to increase in Wyoming in the future and
³⁹⁵ average precipitation is expected to remain relatively constant, we project an increase in sagebrush
³⁹⁶ cover at most core areas across Wyoming. Moreover, projected increases were larger in magnitude
³⁹⁷ than decreases and increases were projected on about four times larger land area (about 45,000 km²)
³⁹⁸ expected to experience increases relative to about 13,000 km² expected to experience decreases,
³⁹⁹ on average). This finding suggests that few core areas are “lost causes” in terms of maintaining
⁴⁰⁰ existing sagebrush cover in the future. Continued conservation of these core areas has the potential
⁴⁰¹ to increase sage-grouse populations in the future because the extent of the landscape with sagebrush
⁴⁰² cover that exceeds the nesting threshold is expected to increase for several core areas (Fig. 8). Even
⁴⁰³ when the threshold is not projected to be exceeded, sagebrush cover is most commonly projected to
⁴⁰⁴ increase. While sagebrush is a key component of sage-grouse habitat, our models do not currently
⁴⁰⁵ consider other factors that can affect habitat quality, including herbaceous vegetation, structure and
⁴⁰⁶ configuration of sagebrush on the landscape, or disturbances (Fedy et al. 2014).

407 The most common climate response across the core areas was a positive effect of temperature on
408 sagebrush performance. This finding is consistent with theoretical and empirical research suggesting
409 that plants at the cold-limited edge of their distribution may benefit from global climate change
410 (Amburgey et al. 2018, Kleinhesselink and Adler 2018, Renwick et al. 2018). The finding is also
411 consistent with results across a broader range of the sagebrush distribution using these same data
412 sources (Rigge et al. 2021). Recent mechanistic modeling across the sagebrush biome also suggests
413 that increases in temperature will benefit sagebrush in high elevation portions of its range, like
414 Wyoming (Palmquist et al. 2021). Palmquist et al. (2021) showed that soil moisture will likely
415 remain adequate under a warming climate in warm, moisture-limited areas. Other studies have
416 also found positive effects of temperature increases at high elevation sagebrush sites, likely due to
417 earlier snowmelt and a longer growing season (Perfors et al. 2003, Harte et al. 2015). Our statistical
418 models appear to reflect these underlying mechanistic explanations at a majority of core areas. A
419 negative effect of increased precipitation combined with a positive effect of temperature could
420 reflect sagebrush responding negatively to late season snow in colder years and positively to earlier
421 snowmelt in warmer years.

422 Climate responses were not uniform across core areas, however. The models showed positive
423 and negative responses to both precipitation and temperature annual anomalies. Opposing effects
424 of weather on sagebrush performance are not uncommon (Renwick et al. 2018, Palmquist et al.
425 2021). Regional, landscape, and local gradients in average climate (Kleinhesselink and Adler 2018),
426 soil conditions (Schlaepfer et al. 2012), and subspecies composition (Rosentreter 2005) can have a
427 strong influence on sagebrush responses to weather and climate.

428 The biggest limitation of our study is that we only quantified the direct effects of climate on
429 sagebrush performance. The indirect effects of climate change and other non-climate related effects
430 might be more influential. In particular, the fire-cheatgrass invasion cycle has been implicated as
431 the major driver of sagebrush loss across most of its historical range. Recent modeling suggests
432 that parts of Wyoming may become more suitable for cheatgrass but that cheatgrass invasion could
433 be limited if disturbances that reduce native grass and shrub cover are limited (Palmquist et al.

434 2021). Hotter and drier conditions in the future will likely increase fire risk throughout Wyoming
435 shrublands, meaning it could be difficult to limit cheatgrass invasion if fires become widespread.
436 Nonetheless, our results corroborate those of Palmquist et al. (2021) by suggesting that climate
437 change alone should benefit, or at least not significantly disadvantage, sagebrush in Wyoming.

438 Our sagebrush projections can be used as part of a decision-support toolbox for managers in
439 Wyoming. The projections are also useful for generating hypotheses and scientific questions. For
440 example, what conditions lead to two core areas in the same region having divergent responses
441 to temperature (North Gillette versus Thunder Basin, Fig. 4A)? Observational and experimental
442 studies could help explain the divergent responses. Such explanations are critical to guide region-
443 wide management of sagebrush landscapes in the face of climate change and potential cheatgrass
444 invasion.

445 Implications for sage-grouse management

446 Sage-grouse are sagebrush-obligate species, meaning any increase in sagebrush cover likely benefits
447 sage-grouse but consideration of other habitat components also affect habitat quality for sage-grouse
448 (Fedy et al. 2014). Although not all core areas are projected to increase in sagebrush cover,
449 the magnitude of increase and the area over which we project increases far outweighs projected
450 declines. These results highlight the importance of active and adaptive management in Wyoming's
451 sage-grouse core areas, which contain about 37% of all sage-grouse (Fedy et al. 2014). Our
452 results suggest that climate change per se is not going to cause declines in sagebrush in Wyoming.
453 Therefore, management actions aimed at reducing cheatgrass invasion and limiting disturbances in
454 core areas might help mitigate the negative, indirect impacts of climate change. In part, this is good
455 news because managing disturbances and plant invasions is more feasible than managing global
456 climate change.

457 Even still, effectively conserving all of the core areas may not be enough. Sage-grouse use vast
458 areas outside of the core areas as well, particularly in the apex of the population cycles (Heinrichs

459 et al. 2019). Sage-grouse require diverse resource compositions across life stages, with an upper
460 limit of annual life-time home ranges estimated at ~2975 km² (Connelly et al. 2000b, Connelly et
461 al. 2000a). This suggests that maintaining large intact landscapes inside and outside of core areas
462 (Heinrichs et al. 2019) can help ensure viable sage-grouse populations persist. Our models help
463 to identify sagebrush habitats that persist into the future given climate change, which should be
464 protected from disturbances. Areas with projected sagebrush declines may need to be more closely
465 managed.

466 Acknowledgements

467 This study was funded by the Bureau of Land Management and the US Geological Survey. Any use
468 of trade, firm, or product names is for descriptive purposes only and does not imply endorsement by
469 the U.S. government. We thank Darren Long for reviewing preliminary versions of the manuscript.

470 References

- 471 Amburgey, S. M., D. A. W. Miller, E. H. C. Grant, T. A. G. Rittenhouse, M. F. Benard, J. L.
472 Richardson, M. C. Urban, W. Hughson, A. B. Brand, C. J. Davis, C. R. Hardin, P. W. C.
473 Paton, C. J. Raithel, R. A. Relyea, A. F. Scott, D. K. Skelly, D. E. Skidds, C. K. Smith, and E.
474 E. Werner. 2018. Range position and climate sensitivity: The structure of among-population
475 demographic responses to climatic variation. *Global Change Biology* 24:439–454.
- 476 Balch, J. K., B. A. Bradley, C. M. D'Antonio, and J. Gómez-Dans. 2013. Introduced annual grass
477 increases regional fire activity across the arid western USA (1980–2009). *Global Change
478 Biology* 19:173–183.
- 479 Boettiger, C., M. Bode, J. N. Sanchirico, J. LaRiviere, A. Hastings, and P. R. Armsworth. 2016.
480 Optimal management of a stochastically varying population when policy adjustment is costly.
481 *Ecological Applications* 26:808–817.

- 482 Bradley, B. A. 2009. Regional analysis of the impacts of climate change on cheatgrass invasion
483 shows potential risk and opportunity. *Global Change Biology* 15:196–208.
- 484 Cardinale, B. J., J. E. Duffy, A. Gonzalez, D. U. Hooper, C. Perrings, P. Venail, A. Narwani,
485 G. M. Mace, D. Tilman, D. A. Wardle, A. P. Kinzig, G. C. Daily, M. Loreau, J. B. Grace,
486 A. Larigauderie, D. S. Srivastava, and S. Naeem. 2012. Biodiversity loss and its impact on
487 humanity. *Nature* 486:59–67.
- 488 Carlisle, J., and A. Chalfoun. 2020. The abundance of Greater Sage-Grouse as a proxy for the
489 abundance of sagebrush-associated songbirds in Wyoming, USA. *Avian Conservation and
490 Ecology* 15.
- 491 Chambers, J. C., B. A. Roundy, R. R. Blank, S. E. Meyer, and A. Whittaker. 2007. What Makes
492 Great Basin Sagebrush Ecosystems Invasive by *Bromus Tectorum*? *Ecological Monographs*
493 77:117–145.
- 494 Clark, J. S., S. R. Carpenter, M. Barber, S. Collins, A. Dobson, J. A. Foley, D. M. Lodge, M.
495 Pascual, R. Pielke, W. Pizer, C. Pringle, W. V. Reid, K. A. Rose, O. Sala, W. H. Schlesinger,
496 D. H. Wall, and D. Wear. 2001. Ecological Forecasts: An Emerging Imperative. *Science*
497 293:657–660.
- 498 Conn, P. B., D. S. Johnson, J. M. V. Hoef, M. B. Hooten, J. M. London, and P. L. Boveng. 2015.
499 Using spatiotemporal statistical models to estimate animal abundance and infer ecological
500 dynamics from survey counts. *Ecological Monographs* 85:235–252.
- 501 Conn, P. B., D. S. Johnson, P. J. Williams, S. R. Melin, and M. B. Hooten. 2018. A guide to
502 Bayesian model checking for ecologists. *Ecological Monographs* 88:526–542.
- 503 Connelly, J. W., S. T. Knick, M. A. Schroeder, and S. J. Stiver. 2000a. Conservation assessment of
504 greater sage-grouse and sagebrush habitats. Western Association of Fish; Wildlife Agencies,
505 Cheyenne, Wyoming.
- 506 Connelly, J. W., K. P. Reese, R. A. Fischer, and W. L. Wakkinen. 2000b. Response of a
507 Sage Grouse Breeding Population to Fire in Southeastern Idaho. *Wildlife Society Bulletin
508 (1973-2006)* 28:90–96.

- 509 Dietze, M. C., A. Fox, L. M. Beck-Johnson, J. L. Betancourt, M. B. Hooten, C. S. Jarnevich,
510 T. H. Keitt, M. A. Kenney, C. M. Laney, L. G. Larsen, H. W. Loescher, C. K. Lunch, B. C.
511 Pijanowski, J. T. Randerson, E. K. Read, A. T. Tredennick, R. Vargas, K. C. Weathers, and
512 E. P. White. 2018. Iterative near-term ecological forecasting: Needs, opportunities, and
513 challenges. *Proceedings of the National Academy of Sciences* 115:1424–1432.
- 514 Edmunds, D. R., C. L. Aldridge, M. S. O'Donnell, and A. P. Monroe. 2018. Greater sage-grouse
515 population trends across Wyoming. *The Journal of Wildlife Management* 82:397–412.
- 516 Eyring, V., S. Bony, G. A. Meehl, C. A. Senior, B. Stevens, R. J. Stouffer, and K. E. Taylor. 2016.
517 Overview of the Coupled Model Intercomparison Project Phase 6 (CMIP6) experimental
518 design and organization. *Geoscientific Model Development* 9:1937–1958.
- 519 Farber, S., R. Costanza, D. L. Childers, J. Erickson, K. Gross, M. Grove, C. S. Hopkinson, J.
520 Kahn, S. Pincetl, A. Troy, P. Warren, and M. Wilson. 2006. Linking Ecology and Economics
521 for Ecosystem Management. *BioScience* 56:121–133.
- 522 Fedy, B. C., K. E. Doherty, C. L. Aldridge, M. O'Donnell, J. L. Beck, B. Bedrosian, D. Gummer,
523 M. J. Holloran, G. D. Johnson, N. W. Kaczor, C. P. Kirol, C. A. Mandich, D. Marshall, G.
524 McKee, C. Olson, A. C. Pratt, C. C. Swanson, and B. L. Walker. 2014. Habitat prioritization
525 across large landscapes, multiple seasons, and novel areas: An example using greater sage-
526 grouse in Wyoming. *Wildlife Monographs* 190:1–39.
- 527 Gelman, A., and J. Hill. 2006. *Data Analysis Using Regression and Multilevel/Hierarchical
528 Models*. Cambridge University Press.
- 529 Gelman, A., and D. B. Rubin. 1992. Inference from Iterative Simulation Using Multiple
530 Sequences. *Statistical Science* 7:457–472.
- 531 Guo, J., J. Gabry, B. Goodrich, S. Weber, D. Lee, K. Sakrejda, M. Martin, T. of C. University, O.
532 Sklyar (R/cxxfunplus.R), T. R. C. Team (R/pairs.R, R/dynGet.R), J. Oehlschlaegel-Akiyoshi
533 (R/pairs.R), J. Maddock (gamma.hpp), P. Bristow (gamma.hpp), N. Agrawal (gamma.hpp),
534 C. Kormanyos (gamma.hpp), and B. Steve. 2020, July. Rstan: R Interface to Stan.
- 535 Harte, J., S. R. Saleska, and C. Levy. 2015. Convergent ecosystem responses to 23-year ambient

- 536 and manipulated warming link advancing snowmelt and shrub encroachment to transient and
537 long-term climate–soil carbon feedback. *Global Change Biology* 21:2349–2356.
- 538 Heinrichs, J. A., M. S. O’Donnell, C. L. Aldridge, S. L. Garman, and C. G. Homer. 2019.
539 Influences of potential oil and gas development and future climate on Sage-grouse declines
540 and redistribution. *Ecological Applications* 29:e01912.
- 541 Hobbs, N. T., and M. B. Hooten. 2015. *Bayesian Models: A Statistical Primer for Ecologists*.
542 Princeton University Press.
- 543 Ives, A. R., B. Dennis, K. L. Cottingham, and S. R. Carpenter. 2003. Estimating Community
544 Stability and Ecological Interactions from Time-Series Data. *Ecological Monographs* 73:301–
545 330.
- 546 Jia, H., and A. Chong. 2020. Epwshiftr: Create Future ‘EnergyPlus’ Weather Files using
547 ‘CMIP6’ Data.
- 548 Kleinhesselink, A. R., and P. B. Adler. 2018. The response of big sagebrush (*Artemisia tridentata*)
549 to interannual climate variation changes across its range. *Ecology* 99:1139–1149.
- 550 McDonald, T., A. M. (HIP. sampling methods), M. Kleinsausser, and S. E. (Auto. testing and
551 Travis). 2020, July. SDraw: Spatially Balanced Samples of Spatial Objects.
- 552 McShane, T. O., P. D. Hirsch, T. C. Trung, A. N. Songorwa, A. Kinzig, B. Monteferri, D.
553 Mutekanga, H. V. Thang, J. L. Dammert, M. Pulgar-Vidal, M. Welch-Devine, J. Peter
554 Brosius, P. Coppolillo, and S. O’Connor. 2011. Hard choices: Making trade-offs between
555 biodiversity conservation and human well-being. *Biological Conservation* 144:966–972.
- 556 Nepstad, D. C., C. M. Stickler, B. S.-. Filho, and F. Merry. 2008. Interactions among Amazon
557 land use, forests and climate: Prospects for a near-term forest tipping point. *Philosophical
558 Transactions of the Royal Society B: Biological Sciences* 363:1737–1746.
- 559 Ogle, K., and J. J. Barber. 2020. Ensuring identifiability in hierarchical mixed effects Bayesian
560 models. *Ecological Applications* 30:e02159.
- 561 Palmquist, K. A., D. R. Schlaepfer, R. R. Renne, S. C. Torbit, K. E. Doherty, T. E. Remington,
562 G. Watson, J. B. Bradford, and W. K. Lauenroth. 2021. Divergent climate change effects

563 on widespread dryland plant communities driven by climatic and ecohydrological gradients.

564 Global Change Biology n/a.

565 Pastick, N. J., B. K. Wylie, M. B. Rigge, D. Dahal, S. P. Boyte, M. O. Jones, B. W. Allred, S.

566 Parajuli, and Z. Wu. 2021. Rapid Monitoring of the Abundance and Spread of Exotic Annual

567 Grasses in the Western United States Using Remote Sensing and Machine Learning. AGU

568 Advances 2:e2020AV000298.

569 Perfors, T., J. Harte, and S. E. Alter. 2003. Enhanced growth of sagebrush (*Artemisia tridentata*)

570 in response to manipulated ecosystem warming. Global Change Biology 9:736–742.

571 Pilliod, D. S., M. I. Jeffries, R. S. Arkle, and D. H. Olson. 2020. Reptiles Under the Conservation

572 Umbrella of the Greater Sage-Grouse. The Journal of Wildlife Management 84:478–491.

573 Powers, R. P., and W. Jetz. 2019. Global habitat loss and extinction risk of terrestrial vertebrates

574 under future land-use-change scenarios. Nature Climate Change 9:323–329.

575 R Core Team. 2020. R: A Language and Environment for Statistical Computing. R Foundation

576 for Statistical Computing.

577 Renwick, K. M., C. Curtis, A. R. Kleinhesselink, D. Schlaepfer, B. A. Bradley, C. L. Aldridge, B.

578 Poulter, and P. B. Adler. 2018. Multi-model comparison highlights consistency in predicted

579 effect of warming on a semi-arid shrub. Global Change Biology 24:424–438.

580 Rigge, M., C. Homer, L. Cleeves, D. K. Meyer, B. Bunde, H. Shi, G. Xian, S. Schell, and

581 M. Bobo. 2020. Quantifying Western U.S. Rangelands as Fractional Components with

582 Multi-Resolution Remote Sensing and In Situ Data. Remote Sensing 12:412.

583 Rigge, M., H. Shi, and K. Postma. 2021. Projected change in rangeland fractional component

584 cover across the sagebrush biome under climate change through 2085. Ecosphere 12:e03538.

585 Rosentreter, R. 2005. Sagebrush identification, ecology, and palatability relative to sage-grouse.

586 In: Shaw, Nancy L.; Pellatt, Mike; Monsen, Stephen B., comps. 2005. Sage-grouse habitat

587 restoration symposium proceedings; 2001 June 4-7, Boise, ID. Proc. RMRS-P-38. Fort

588 Collins, CO: U.S. Department of Agriculture, Forest Service, Rocky Mountain Research

589 Station. p. 3-16 038.

- 590 Rowland, M. M., M. J. Wisdom, L. H. Suring, and C. W. Meinke. 2006. Greater sage-grouse as
591 an umbrella species for sagebrush-associated vertebrates. *Biological Conservation* 129:323–
592 335.
- 593 Rupp, D. E., J. T. Abatzoglou, K. C. Hegewisch, and P. W. Mote. 2013. Evaluation of CMIP5
594 20th century climate simulations for the Pacific Northwest USA. *Journal of Geophysical
595 Research: Atmospheres* 118:10, 884–10, 906.
- 596 Sala, O. E., F. S. Chapin, Iii, J. J. Armesto, E. Berlow, J. Bloomfield, R. Dirzo, E. Huber-Sanwald,
597 L. F. Huenneke, R. B. Jackson, A. Kinzig, R. Leemans, D. M. Lodge, H. A. Mooney, M.
598 Oesterheld, N. L. Poff, M. T. Sykes, B. H. Walker, M. Walker, and D. H. Wall. 2000. Global
599 Biodiversity Scenarios for the Year 2100. *Science* 287:1770–1774.
- 600 Schlaepfer, D. R., W. K. Lauenroth, and J. B. Bradford. 2012. Ecohydrological niche of
601 sagebrush ecosystems. *Ecohydrology* 5:453–466.
- 602 Smith, I. T., J. L. Rachlow, L. K. Svancara, L. A. McMahon, and S. J. Knetter. 2019. Habitat
603 specialists as conservation umbrellas: Do areas managed for greater sage-grouse also protect
604 pygmy rabbits? *Ecosphere* 10:e02827.
- 605 Stan Development Team. 2020. Stan Modeling Language Users Guide and Reference Manual,
606 2.12.2.
- 607 Stiver, S. J., E. T. Rinkes, D. E. Naugle, P. D. Makela, D. A. Nance, and J. W. Karl. 2015.
608 Sage-grouse Habitat Assessment Framework: A Multiscale Assessment Tool. Technical
609 Reference 6710-1. Bureau of Land Management; Western Association of Fish; Wildlife
610 Agencies, Denver, Colorado.
- 611 Tredennick, A. T., M. B. Hooten, C. L. Aldridge, C. G. Homer, A. R. Kleinhesselink, and P. B.
612 Adler. 2016. Forecasting climate change impacts on plant populations over large spatial
613 extents. *Ecosphere* 7:e01525.
- 614 Walters, C. J., and R. Hilborn. 1978. Ecological Optimization and Adaptive Management.
615 Annual Review of Ecology and Systematics 9:157–188.

List of Figures

617	1	Observed time series of percent cover for each core area from the Back-In-Time product. Line shows mean cover in each year across all cells (pixels). The shaded region shows the mean plus/minus the standard deviation across all cells (pixels) in each year. Note that the y-axis changes across panels.	29
621	2	(A) Relative errors of global circulation models when comparing historical projections to observed PRISM climate data within Wyoming sage-grouse core areas for the period 1985-2018. Values in the top panel (Combined) were subtracted from 1 and normalized for use as model weights when projecting sagebrush dynamics. GCMs are ordered from lowest (left) to highest (right) combined error. (B) Climate change projections for Greater South Pass (north) from all GCMs (light lines) and the weighted average of climate projections, which are proportional to the relative errors in panel A.	30
629	3	Posterior distributions of equilibrium cover calculated from fitted model parameters. The vertical black lines show the observed mean cover for each core area from 1985-2018.	31
632	4	Sensitivity of sagebrush cover to temperature and precipitation. Maps show the mean of the posterior distribution of sensitivity to temperature (A) and precipitation (B) for each core area. Panels to the right of the maps show the mean (crosshairs), 95% Bayesian credible interval (bold lines), and range of the posterior distributions (whiskers) of sensitivity to temperature (C) and precipitation (D) for each core area. Colors indicate positive (greens), negative (browns), and negligible (light grey) sensitivity. Sensitivity is defined as the log change in cover relative to equilibrium cover when a +1 standard deviation perturbation is applied to the climate effect in the fitted model for each core area.	32
641	5	Sensitivity of each core area to temperature and precipitation grouped by positive and negative responses to each climate driver. (A) Core areas with negative sensitivity to precipitation and positive sensitivity to temperature. (B) Core areas with positive sensitivity to precipitation and temperature, (C) Core areas with a negative sensitivity to precipitation and temperature. (D) Core areas with a positive sensitivity to precipitation and a negative sensitivity to temperature. Points show the posterior means and whiskers show the 95% Bayesian credible intervals. Dashed tan lines show where sensitivity equals zero. The panel labels also indicate the number of core areas (n) in each sensitivity quadrant.	33
650	6	Projections of sagebrush percent cover from 2018 to 2080 under three climate change scenarios (ssp indicated by colors) for each core area. The solid line is the median of the posterior predictive distribution; light shaded ribbon bounds the 68% BCI; very light shaded ribbon bounds the 95% BCI. Box and whiskers show the 68% (boxes) and 95% (whiskers) BCIs at discrete time horizons of 2020, 2040, 2060, and 2080. The y-axis scale differs across plots.	34

656	7	Projections of sagebrush percent cover (color bars indicate percent cover value) over space and time for the Salt Wells (SlW) core area. Projections are plotted from a single ensemble member (one parameter set) and using the ssp585 climate forcing scenario.	35
660	8	Projections of the proportion of 100-meter cells within a core area where sagebrush percent cover exceeds the sage-grouse nesting threshold defined for each core area. The solid line is the median of the posterior predictive distribution; light shaded ribbon bounds the 68% BCI; very light shaded ribbon bounds the 95% BCI. The dashed horizontal line shows where the proportion of cells is equal to 50% of the area. The y-axis scale differs across plots.	36
666	9	Sage-grouse population growth rates from Edmunds et al. (2018) for each core area, grouped by whether (A) the core area is currently more suitable and projected to remain more suitable, (B) currently more suitable and projected to become less suitable, (C) currently less suitable and projected to remain less suitable, and (D) currently less suitable and projected to become more suitable. ‘More suitable’ is defined as over 50% of cells with cover over the nesting threshold. ‘Less suitable’ is defined as fewer than 50% of cells with cover over the nesting threshold.	37
672			

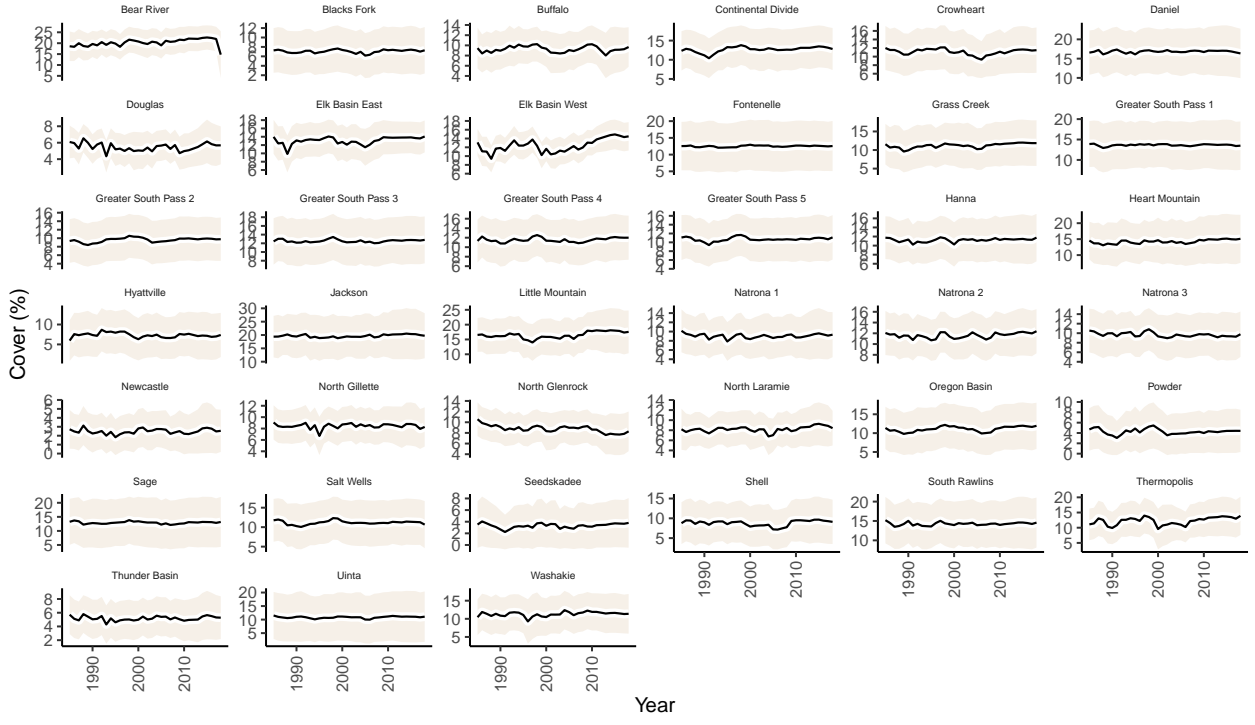


Figure 1: Observed time series of percent cover for each core area from the Back-In-Time product. Line shows mean cover in each year across all cells (pixels). The shaded region shows the mean plus/minus the standard deviation across all cells (pixels) in each year. Note that the y-axis changes across panels.

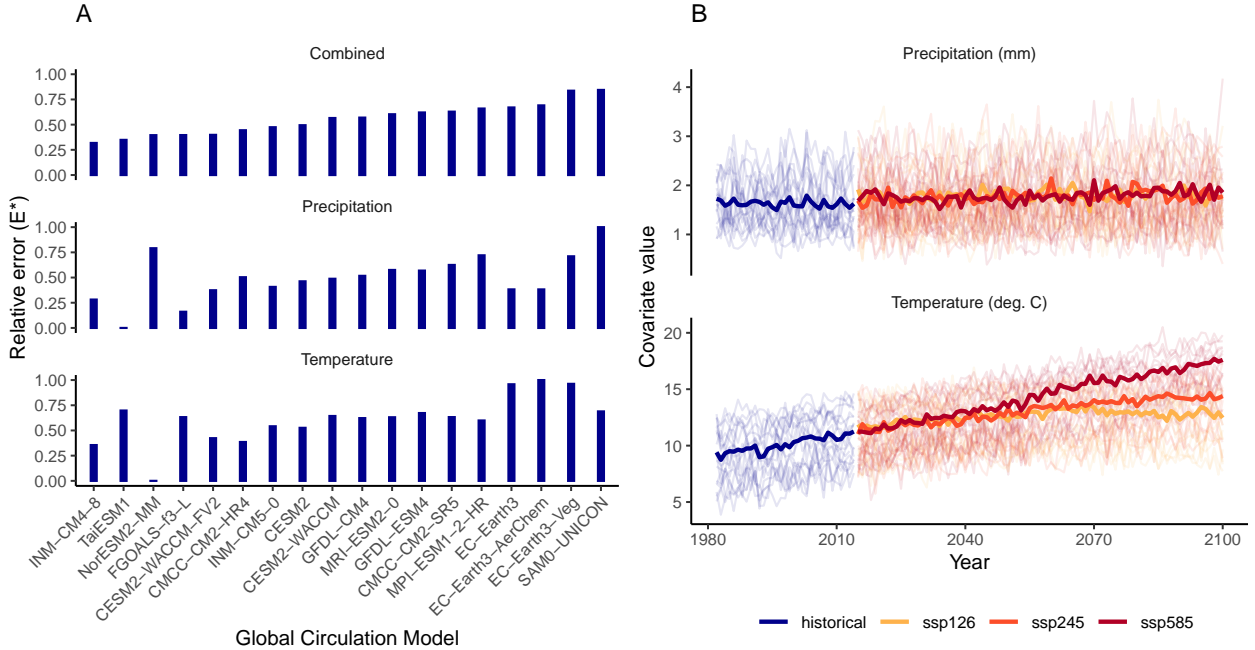


Figure 2: (A) Relative errors of global circulation models when comparing historical projections to observed PRISM climate data within Wyoming sage-grouse core areas for the period 1985-2018. Values in the top panel (Combined) were subtracted from 1 and normalized for use as model weights when projecting sagebrush dynamics. GCMs are ordered from lowest (left) to highest (right) combined error. (B) Climate change projections for Greater South Pass (north) from all GCMs (light lines) and the weighted average of climate projections, which are proportional to the relative errors in panel A.

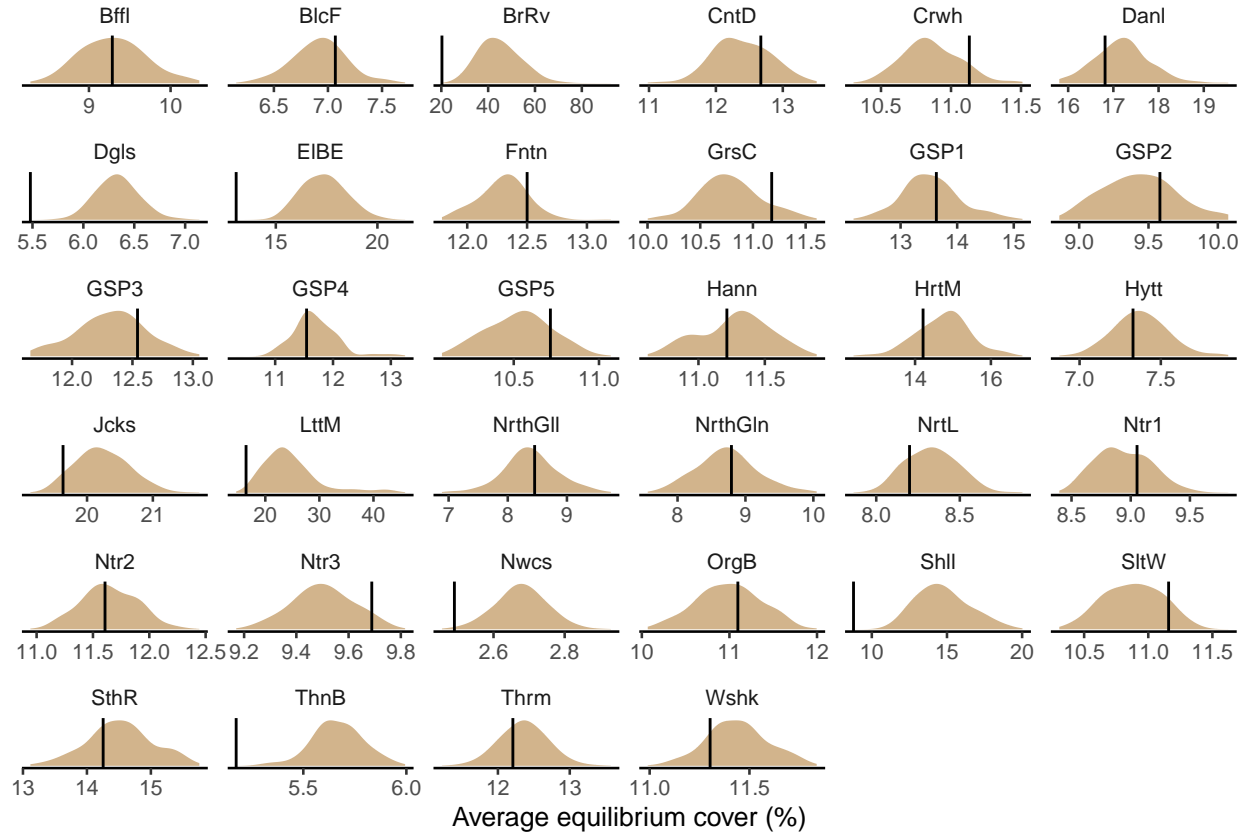


Figure 3: Posterior distributions of equilibrium cover calculated from fitted model parameters. The vertical black lines show the observed mean cover for each core area from 1985-2018.

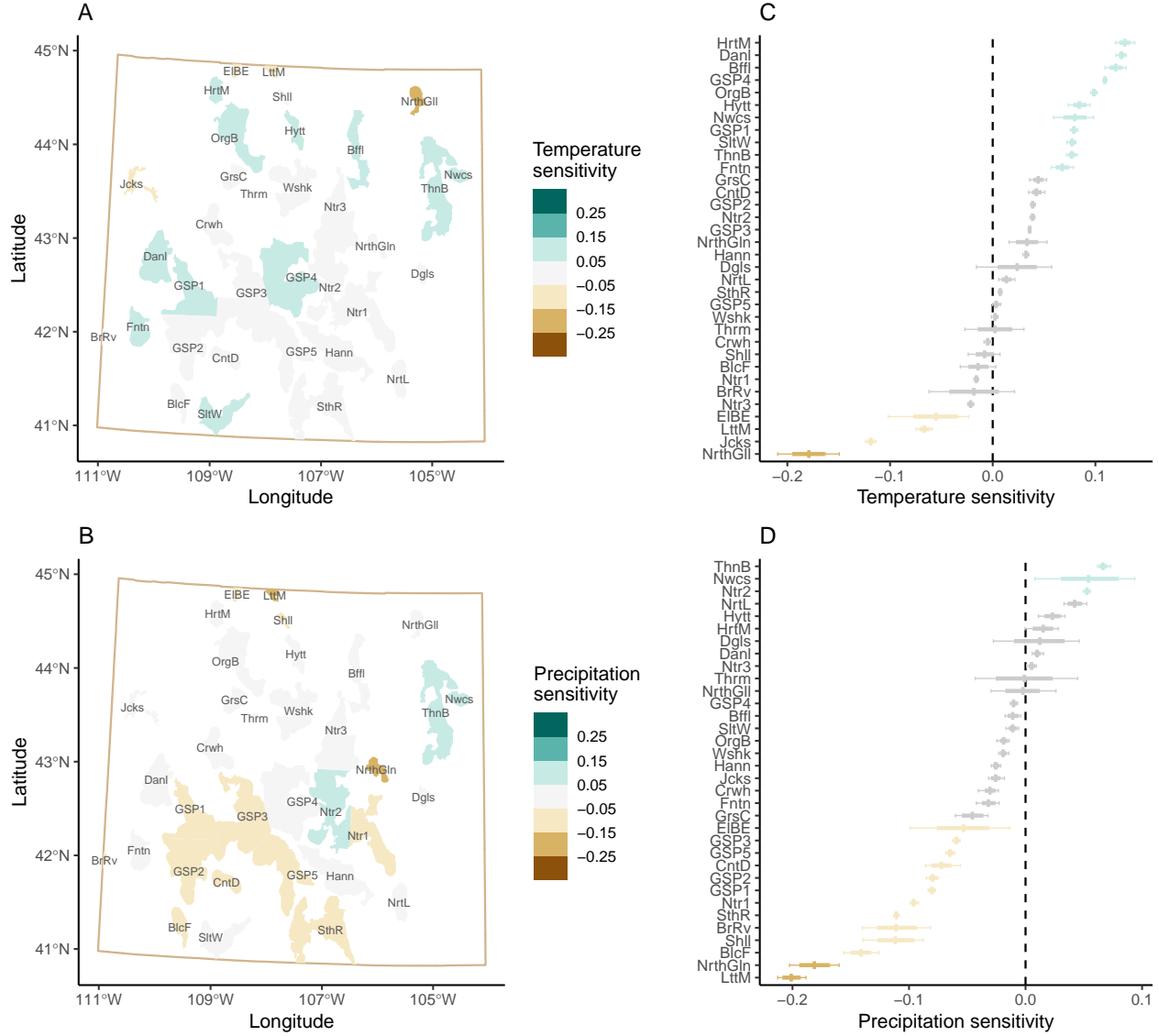


Figure 4: Sensitivity of sagebrush cover to temperature and precipitation. Maps show the mean of the posterior distribution of sensitivity to temperature (A) and precipitation (B) for each core area. Panels to the right of the maps show the mean (crosshairs), 95% Bayesian credible interval (bold lines), and range of the posterior distributions (whiskers) of sensitivity to temperature (C) and precipitation (D) for each core area. Colors indicate positive (greens), negative (browns), and negligible (light grey) sensitivity. Sensitivity is defined as the log change in cover relative to equilibrium cover when a +1 standard deviation perturbation is applied to the climate effect in the fitted model for each core area.

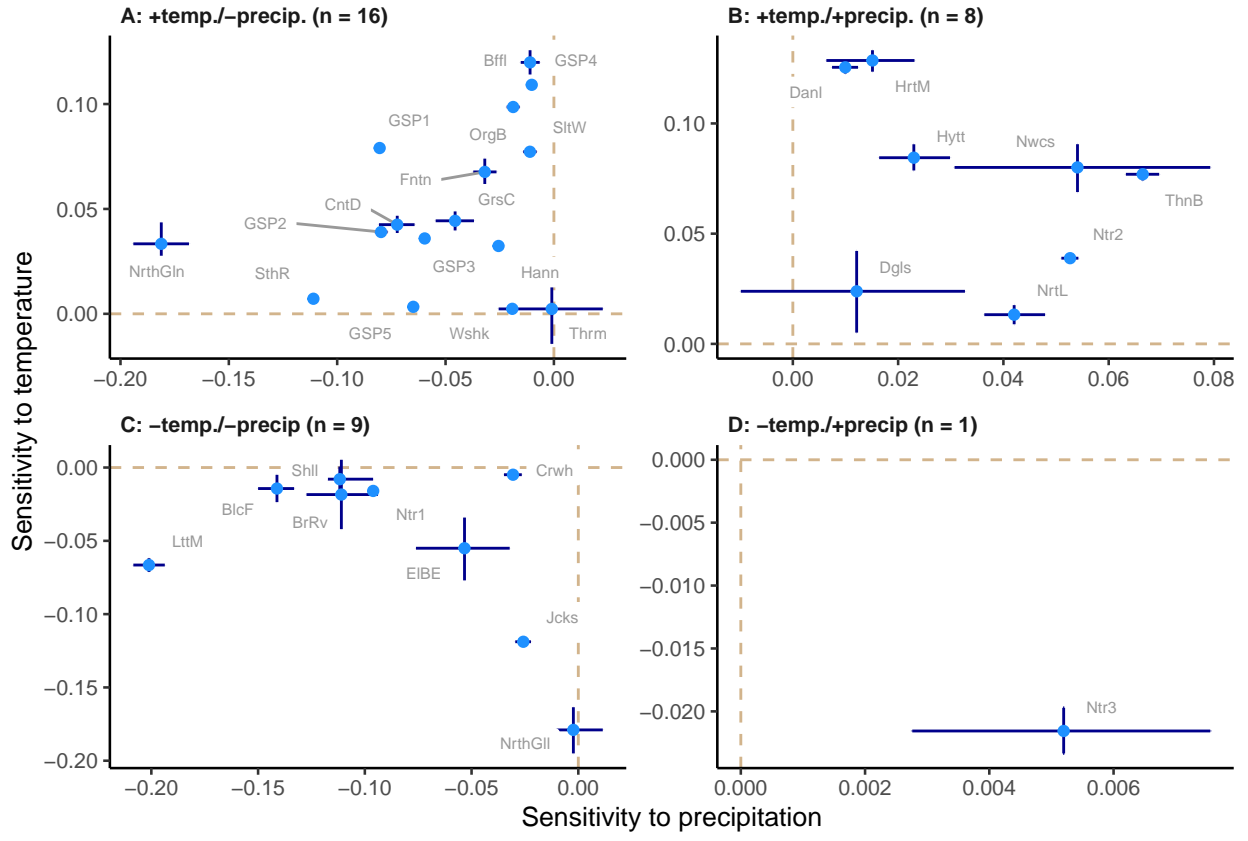


Figure 5: Sensitivity of each core area to temperature and precipitation grouped by positive and negative responses to each climate driver. (A) Core areas with negative sensitivity to precipitation and positive sensitivity to temperature. (B) Core areas with positive sensitivity to precipitation and temperature, (C) Core areas with a negative sensitivity to precipitation and temperature. (D) Core areas with a positive sensitivity to precipitation and a negative sensitivity to temperature. Points show the posterior means and whiskers show the 95% Bayesian credible intervals. Dashed tan lines show where sensitivity equals zero. The panel labels also indicate the number of core areas (n) in each sensitivity quadrant.

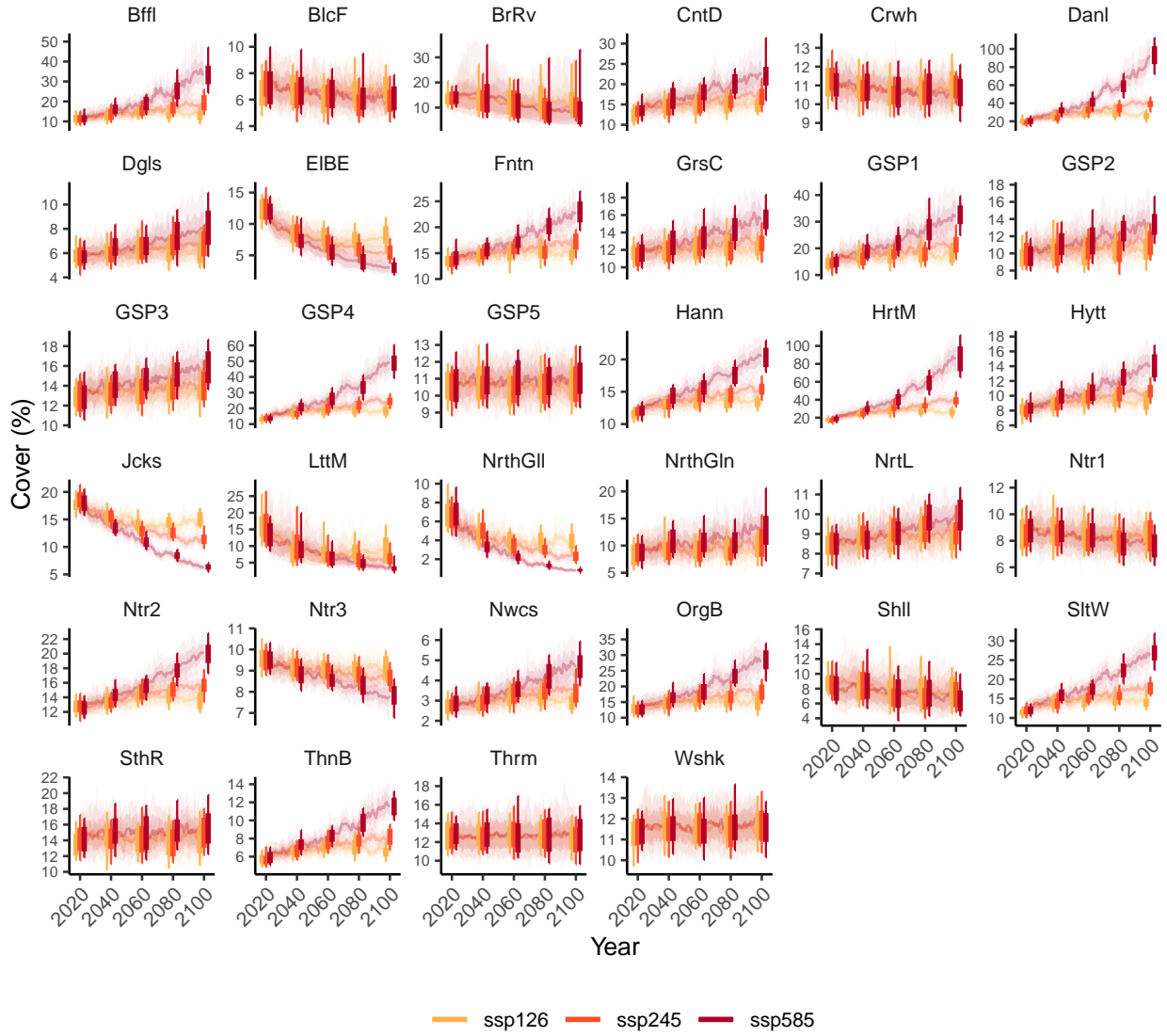


Figure 6: Projections of sagebrush percent cover from 2018 to 2080 under three climate change scenarios (ssp indicated by colors) for each core area. The solid line is the median of the posterior predictive distribution; light shaded ribbon bounds the 68% BCI; very light shaded ribbon bounds the 95% BCI. Box and whiskers show the 68% (boxes) and 95% (whiskers) BCIs at discrete time horizons of 2020, 2040, 2060, and 2080. The y-axis scale differs across plots.

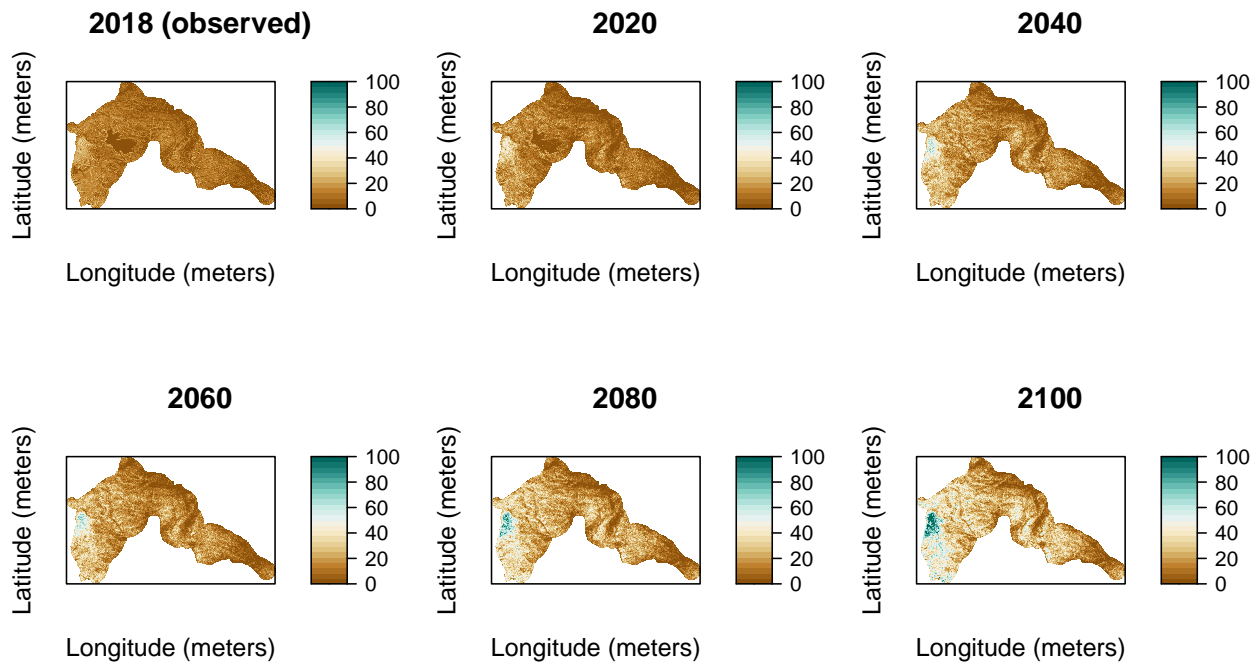


Figure 7: Projections of sagebrush percent cover (color bars indicate percent cover value) over space and time for the Salt Wells (SltW) core area. Projections are plotted from a single ensemble member (one parameter set) and using the ssp585 climate forcing scenario.

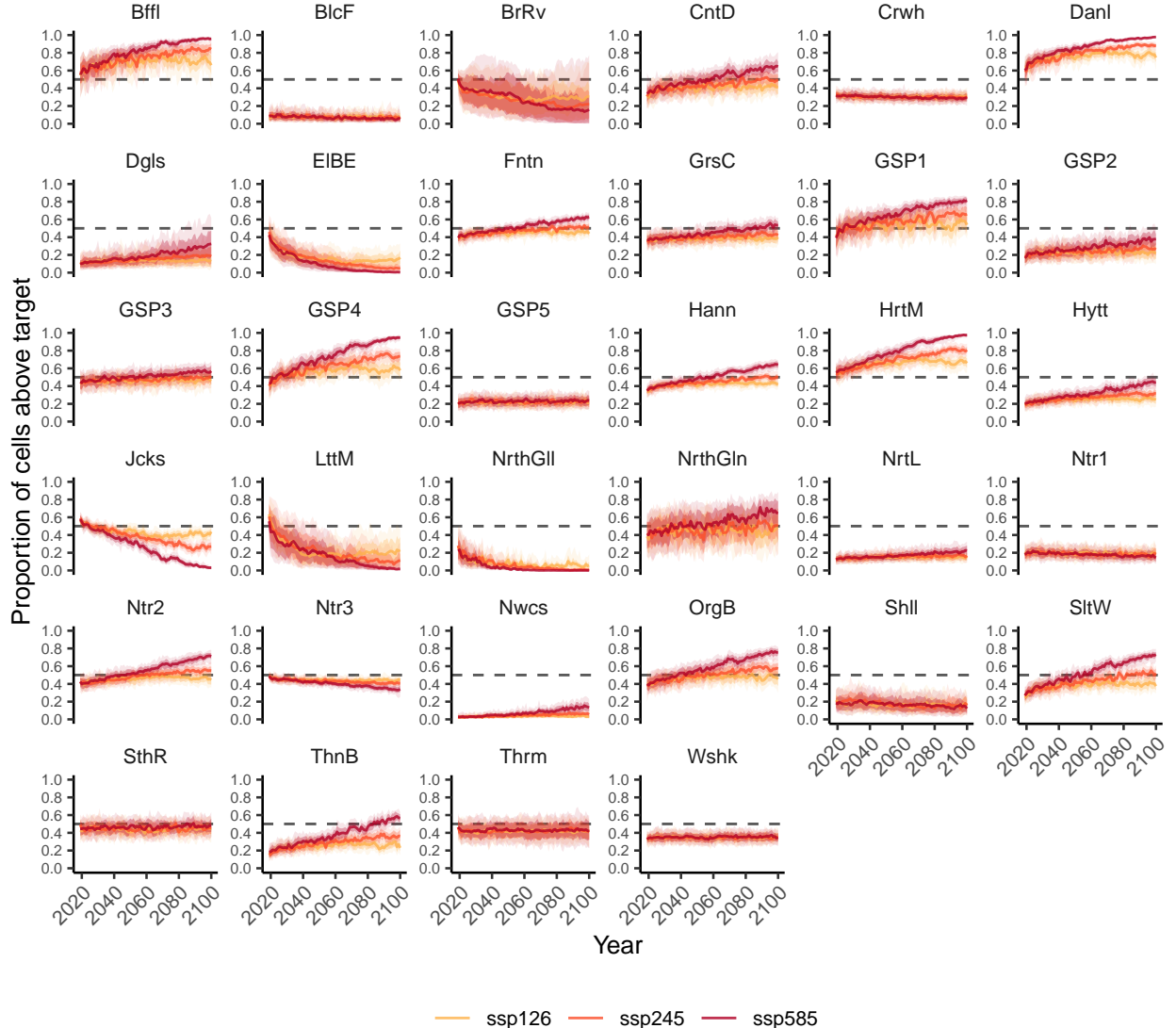


Figure 8: Projections of the proportion of 100-meter cells within a core area where sagebrush percent cover exceeds the sage-grouse nesting threshold defined for each core area. The solid line is the median of the posterior predictive distribution; light shaded ribbon bounds the 68% BCI; very light shaded ribbon bounds the 95% BCI. The dashed horizontal line shows where the proportion of cells is equal to 50% of the area. The y-axis scale differs across plots.

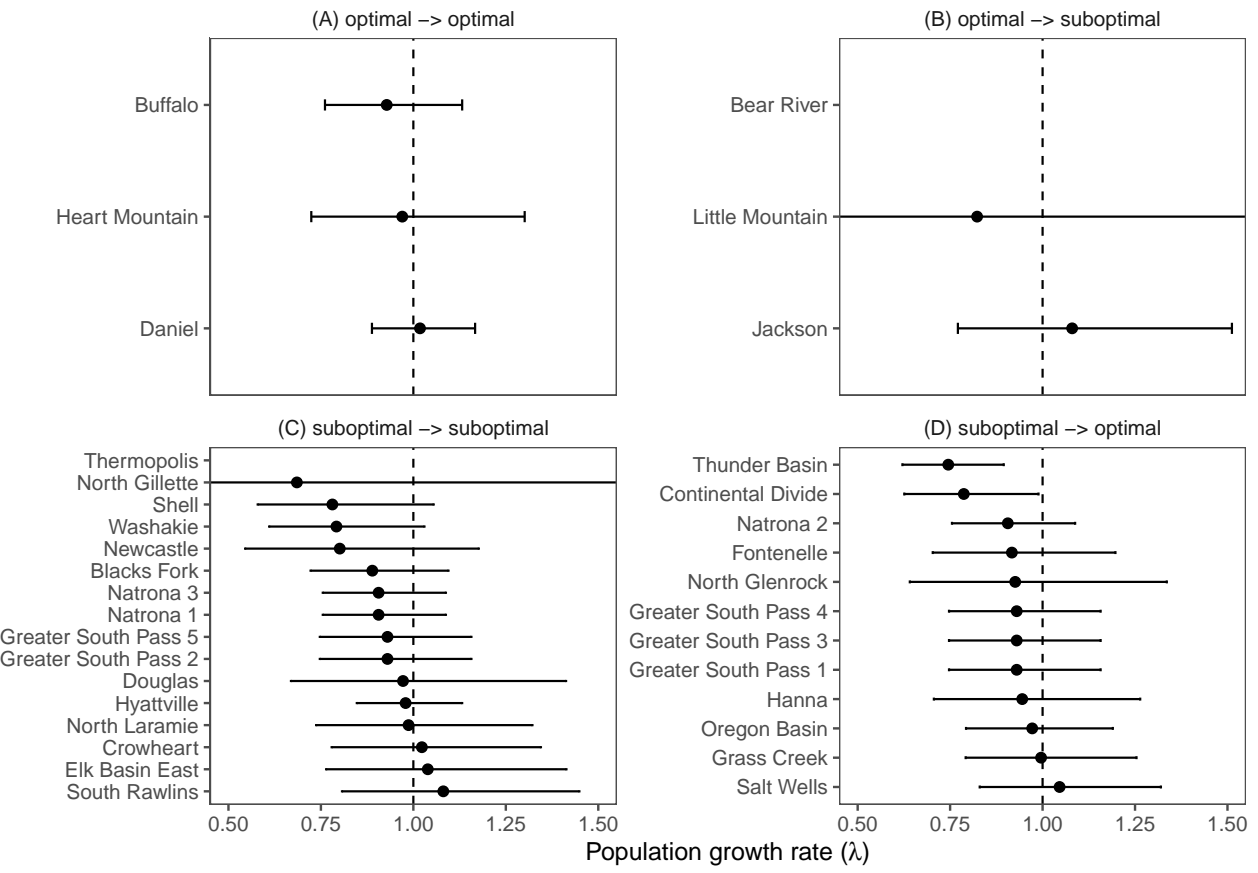


Figure 9: Sage-grouse population growth rates from Edmunds et al. (2018) for each core area, grouped by whether (A) the core area is currently more suitable and projected to remain more suitable, (B) currently more suitable and projected to become less suitable, (C) currently less suitable and projected to remain less suitable, and (D) currently less suitable and projected to become more suitable. ‘More suitable’ is defined as over 50% of cells with cover over the nesting threshold. ‘Less suitable’ is defined as fewer than 50% of cells with cover over the nesting threshold.

List of Tables

674	1	Prior distributions for the dynamic-additive spatiotemporal regression model of sagebrush cover.	39
675	2	Averages and variances of climate covariates over different time periods. Averages are average values over the core areas. Core area values were the weighted averages according to GCM weights. Variances are average variances over the core areas. Core area variances were computed over the weighted averages of values for each core area.	40
676	3	Results from colonization model for each core area. $\text{Pr}(\text{colonize} \mid \text{cover} = 0)$ reads, 'the probability of colonization given that current cover is zero.'	41
677			
678			
679			
680			
681			
682			

Table 1: Prior distributions for the dynamic-additive spatiotemporal regression model of sagebrush cover.

Parameter	Definition	Distribution	Source
β_1	intercept	Normal(0.73, 1)	Tredennick et al. (2016)
β_2	density-dependence	Normal(0.72, 1)	Tredennick et al. (2016)
$\beta_{3\&4}$	effects of precipitation (β_3) and temperature (β_4)	Normal(0, 5)	–
γ	temporal random effects	Normal(0, σ_γ)	–
σ_γ	standard deviation of temporal random effects	Cauchy(0, 2.5)	–

Table 2: Averages and variances of climate covariates over different time periods. Averages are average values over the core areas. Core area values were the weighted averages according to GCM weights. Variances are average variances over the core areas. Core area variances were computed over the weighted averages of values for each core area.

GCM Scenario	Time Period	Avg. Precip. (mm)	Var. Precip.	Avg. Temp. (deg. C)	Var. Temp.
historical	Historical	2.027	0.007	11.483	0.456
ssp126	2020 - 2040	2.215	0.016	13.391	0.088
ssp126	2040 - 2060	2.276	0.016	13.989	0.080
ssp126	2060 - 2080	2.266	0.026	14.367	0.069
ssp126	2080 - 2100	2.280	0.013	14.020	0.089
ssp245	2020 - 2040	2.154	0.012	13.157	0.112
ssp245	2040 - 2060	2.229	0.019	14.070	0.236
ssp245	2060 - 2080	2.254	0.020	14.943	0.076
ssp245	2080 - 2100	2.267	0.023	15.419	0.041
ssp585	2020 - 2040	2.149	0.016	13.521	0.247
ssp585	2040 - 2060	2.202	0.012	14.920	0.430
ssp585	2060 - 2080	2.266	0.019	16.699	0.230
ssp585	2080 - 2100	2.284	0.018	18.014	0.229

Table 3: Results from colonization model for each core area. $\text{Pr}(\text{colonize} \mid \text{cover} = 0)$ reads, 'the probability of colonization given that current cover is zero.'

Core area	$\text{Pr}(\text{colonize} \mid \text{cover} = 0)$	Mean cover in colonized cells
Bear River	0.35	3
Blacks Fork	0.14	2
Buffalo	0.35	2
Continental Divide	0.22	2
Crowheart	0.21	2
Daniel	0.22	2
Douglas	0.37	2
Elk Basin East	0.42	2
Fontenelle	0.17	2
Grass Creek	0.15	2
Greater South Pass 1	0.17	2
Greater South Pass 2	0.14	2
Greater South Pass 3	0.18	2
Greater South Pass 4	0.23	2
Greater South Pass 5	0.13	2
Hanna	0.21	2
Heart Mountain	0.31	2
Hyattville	0.18	2
Jackson	0.42	4
Little Mountain	0.43	3
Natrona 1	0.21	2
Natrona 2	0.30	2
Natrona 3	0.19	2
Newcastle	0.19	2
North Gillette	0.17	2
North Glenrock	0.28	3
North Laramie	0.38	3
Oregon Basin	0.19	2
Salt Wells	0.20	2
Shell	0.19	2
South Rawlins	0.39	3
Thermopolis	0.26	3
Thunder Basin	0.24	2
Washakie	0.36	3